Transport and behaviour of water in oil paintings

Duivenvoorden, J.R.

Publication date
2025

Chapter 5 Nanoconfined water clusters in zinc white oil paint

This chapter is based on:
Jorien R. Duivenvoorden, Federico Caporaletti, Sander Woutersen, Katrien Keune and Joen J. Hermans
The Journal of Physical Chemistry C 127(38), **2023**, 19269-19277

Abstract

Pigments in oil paint are bound by a complex oil polymer network, which is prone to water-related chemical degradation. We use cryo-Fourier-transform infrared spectroscopy and differential scanning calorimetry to study how water distributes inside zinc white oil paint. By measuring water freezing and melting transitions, we show that water-saturated zinc white oil paint contains both liquid-like clustered water and non-clustered water. A comparison to titanium white paint and non-pigmented model systems indicates that water clustering happens near the pigment-polymer interface. The cluster size was estimated in the nanometre range based on the ice melting and freezing temperature and on the position of the O-D vibration band. As liquid-like water can play a crucial role in the dissolution and transport of ions and molecules, understanding the factors that favour this phenomenon is essential for establishing safe conditions for conservation of painted works of art.

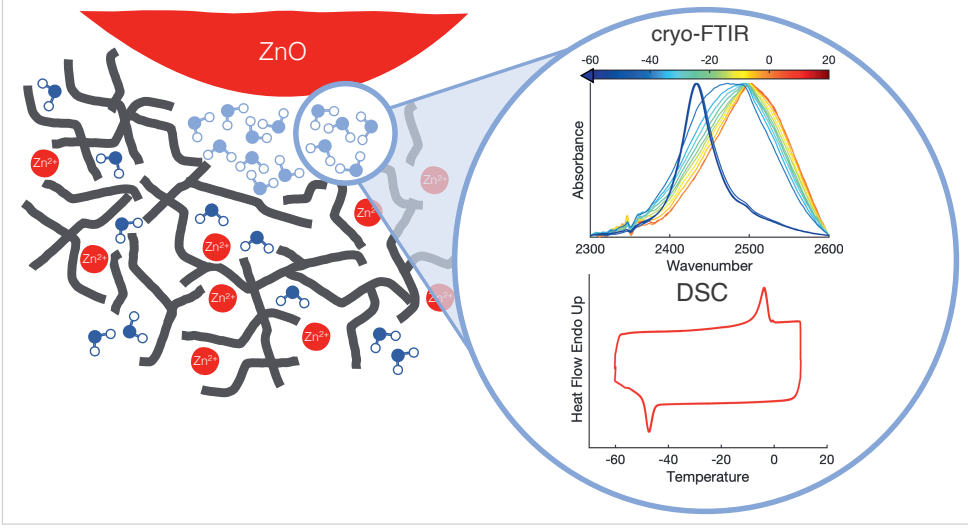

5.1 Introduction

The behaviour and distribution of water in non-hydrophilic environments is an important research topic, for instance in the study of membranes and proteins, nanotubes, organic frameworks and (super) hydrophobic coatings [1], [2], [3], [4], [5]. Especially in the barrier coating industry, clustering of water in liquid-like droplets has huge implications for the properties and performance of a coating, because the presence of water clusters influences the water diffusion rate, plasticization, and corrosion reactions on metal substrates [6], [7], [8], [9], [10], [11]. Additionally, research on rubbers has shown that water inside hydrophobic elastomers such as rubber is distributed as nanoscale droplets [12], [13], [14]. Here, we introduce historical oil paint as a material where water clustering may have a great influence on material properties and deterioration rates.

Oil paint has been used to create works of art for many centuries [15]. Fresh oil paint is a suspension of pigment particles in a liquid drying oil such as linseed oil, which itself is a mixture of triglycerides. As a result of oxygen-induced radical auto-oxidation reactions of the unsaturated fatty esters the oil binder cures and forms a complex, cross-linked polymer network [16]. Through oxidation and hydrolysis reactions during paint curing and ageing, the oil paint polymer network gains polar functional groups such as alcohols, aldehydes, ketones, carboxylic acids and metal carboxylates, and the polymer network may generate free fatty acids [17], [18], [19], [20], [21], [22], [23]. Depending on factors such as pigment type and paint age, the chemical properties of oil paint may vary wildly. In general, though, oil paint has a rather low water diffusion coefficient (in the order of 10^{-13} m^2/s) and a low water sorption capacity (ranging between 1 and 10 wt% with a few exceptions) [24], [25], [26], [27], [28].

In this work, we investigate the distribution of water inside zinc white (ZnO) oil paint, famous for its use by artists like Mondriaan, Picasso and Pollock in the 19th and 20th century, and prone to water-related chemical deterioration [20], [29], [30], [31], [32]. Zinc white oil paint forms an ionomeric polymer network upon curing, where zinc ions are bound to carboxylate groups on the polymer backbone that form during paint drying [33]. Of particular concern for the preservation of works of art painted with zinc white is the reaction between free fatty acids and zinc ions that leads to the formation of crystalline zinc soaps [32]. Recent work indicates that the formation and crystallisation kinetics of zinc soaps are strongly influenced by the presence of water [34], [35], [36]. Water may enter the oil paint via humidity in the environment or water-based cleaning and consolidation solutions used in conservation treatments.

We hypothesise that the presence of liquid-like water clusters, as opposed to molecularly distributed water, can open up the possibility of aqueous chemistry inside oil paint layers. For instance, small liquid water domains could play a crucial role in the dissolution and transport of ions and small molecules, processes that stand at the basis of many types of pigment and polymer degradation in oil paint. Therefore, understanding the factors that favour the presence of clustered water and gaining insight into the location of those clusters inside oil paint is hugely relevant for elucidating chemical degradation pathways and the development of safe conservation treatments and storage conditions.

Thus far, only two studies have yielded some information on the distribution of water inside oil paint, both focusing on lead white oil paint [26], [37]. Using nuclear magnetic resonance spectroscopy and low-frequency dielectric spectroscopy, these reports found indirect evidence that hints at water clustering into liquid domains at high humidity conditions. In our work, the

distribution of water was studied by measuring freezing and melting transitions of water absorbed in zinc white oil paint with differential scanning calorimetry (DSC), commonly used for hydrophilic polymers such as hydrogels to distinguish between bulk and confined water [38], [39], [40], [41], [42], [43]. To obtain more information about the environment of water inside zinc white oil paint, we performed complementary isotope-diluted transmission cryo-Fourier-transform infrared (cryo-FTIR) spectroscopy. Isotope-dilution avoids the overlap of symmetric and asymmetric stretch vibrations of water and therefore allows the analysis of the uncoupled O-D stretch vibration in HDO (ν_s(OD), 2300-2600 cm^{-1}), which changes in shape and intensity during the water-ice transition [44], [45], [46], [47].

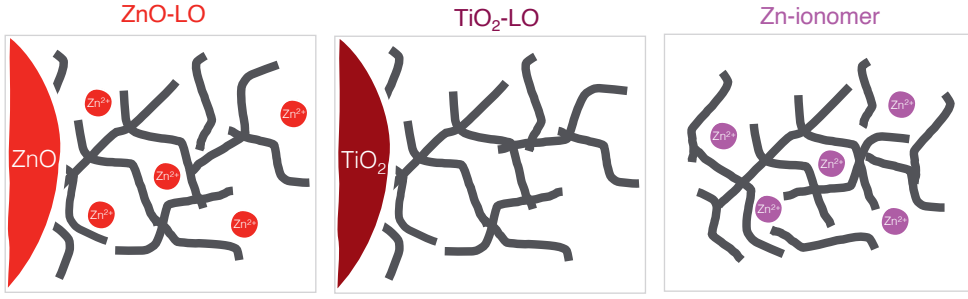

Figure 5.1 Schematic representations of the three systems compared in this work: zinc white linseed oil paint (ZnO-LO), titanium white linseed oil paint (TiO_2-LO) and zinc-ionomer system (Zn-ionomer). The grey lines represent the backbone of the polymerised oil network.

Three types of oil paint model systems were investigated: zinc white linseed oil paint (ZnO-LO), titanium white linseed oil paint (TiO_2-LO) and zinc ionomer (Zn-ionomer). Illustrations of these systems are shown in **Figure 5.1**. The comparison of these three paint systems allows the investigation of the influence of suspended pigment particles and metal ions in the polymer network on the water distribution. Both ZnO-LO and TiO_2-LO contain pigment particles (zinc oxide and titanium dioxide, respectively), where ZnO-LO forms an ionomeric network and TiO_2-LO does not. Zn-ionomer simulates the ionomeric binding medium in zinc white oil paint that surrounds the pigment particles. More details on the characterisation of the zinc ionomer model systems can be found elsewhere [25], [33]. In the following sections the results of the DSC and cryo-FTIR analysis will be discussed and their consequences for oil paint reactivity.

5.2 Materials and methods

Sample preparation

Zinc white (ZnO-LO) and titanium white (TiO_2-LO) oil paints were prepared in a 1:1 w/w pigment:oil ratio. Using a glass muller on a glass slab, 0.102 g zinc oxide (ZnO) (Aldrich, nanopowder, <100 nm particle size) was mixed in 0.11 mL linseed oil (LO) (Kremer Pigmente, from Sweden, cold-pressed, low acid content) and 0.513 mg titanium dioxide (TiO_2) (Huntsman, coated rutile, ± 240 nm particle size) in 0.55 mL linseed oil. This concentration corresponds to pigment volume ratios below the critical pigment volume ratios that are generally reported for zinc white and titanium white oil paints (15 and 20 wt% oil, respectively). Both paints were applied on glass slides using a drawdown bar (30 and 90 µm thickness) and left to cure for 7 days at 60 °C and 12% RH in the dark. The preparation procedure for the

zinc-ionomer model systems was as described by Baij et al. [25], see additional details in **Appendix 5.A**. To obtain water-saturated paint samples, small pieces of paint film (1 x 1 cm) were submerged in deionised water for 2-3 days. A set of ZnO-LO (90 µm thickness) paint films was exposed to a 90% relative humidity environment for 5 days.

Differential scanning calorimetry

A Perkin Elmer Jade differential scanning calorimeter (DSC) was used for this study. The temperature programme cycled twice between 10 and -60 °C with a rate of 5 °C/min. Paint films (90 µm thickness) were taken out of the water, patted dry with paper tissue before being cut into small pieces and placed into sealed aluminium DSC pans. The pans were weighed when empty and after adding the sample on a Sartorius M2P microbalance. To minimise water evaporating from potentially leaking pans, the nitrogen flow in the DSC instrument was turned off during measurements. The aluminium pans were weighed again after the measurement run to check for water evaporation (see **Table 5.A.4** in **Appendix 5.A**).

Transmission cryo-Fourier transform infrared spectroscopy

For transmission cryo-Fourier-transform infrared (cryo-FTIR) spectroscopy, paint films (30 µm thickness) were left 2-3 days in a 10-30% D_2O (Aldrich, 99.9 atom% D) in deionised H_2O solution. The films were taken out of the water, patted dry with paper tissue, and placed between two CaF_2 windows. The temperature of the sample during the measurements was controlled using a liquid-nitrogen cryostat (Optistat DN, Oxford Instruments). The sample chamber was filled with 1 bar of helium to ensure rapid and complete thermalisation. The temperature of the sample was measured using a PT100 thermocouple. The FTIR spectra were recorded in transmission using a Perkin-Elmer Spectrum-Two FTIR spectrometer with a spectral resolution of 4 cm^{-1}. The sample was cooled with a rate of 5 °C/min and measurements were collected every 30 (averaged of 2 spectra) or 90 seconds (average of 8 spectra). The data processing procedure (normalisation and background correction) varied slightly per sample and is indicated in the figure captions.

Transmission Fourier-transform infrared spectroscopy

Supporting measurements were performed using transmission Fourier-transform infrared (FTIR) spectroscopy at room temperature on a Frontier spectrometer (Perkin Elmer). Individual spectra were collected as a single scan and at 4 cm^{-1} resolution. The paint films (30 µm thickness) were placed directly in the infrared beam path without calcium fluoride windows by taping the films over the hole in a metal plate. The data processing details (normalisation and background correction) are indicated in the figure caption.

Dynamic vapour sorption

Dynamic vapour sorption (DVS) analysis was performed using an automatic multi-sample moisture sorption analyzer (SPSx- 11m, Projekt Messtechnik). The relative humidity (RH) inside the climatic chamber was conditioned by mixing a dry nitrogen gas flow with a gas flow saturated with water. The mass increase of the samples was measured with a 10-minute interval on a microbalance (WXS206SDU, MettlerToledo). The samples (90 µm thickness) were subjected to an initial drying step at 0% RH for 300 h before the start of the sorption experiment. The RH was varied in 10% steps every 50 h up to 90% with a final step between 90% and 95% at 22 °C. Equilibrium sorption was assumed to have been reached when there was no mass change of >0.001% over a period of 60 minutes or a maximum step time of 50 hours.

5.3 Results and discussion

DSC measurements on water-saturated paint films

Films of cured oil paint were placed in water until they reached saturation. Sorption isotherms of the oil paint films can be found in **Figure 5.A.1** in **Appendix 5.A**. Freezing and melting transition data are reported in **Table 5.A.1**. The thermogram of ZnO-LO (**Figure 5.2**) showed two types of freezing transitions: a broad freezing peak with an onset at approximately -43 °C and several sharp peaks in the region of -20 to -35 °C. This latter region is similar to where supercooled bulk water freezes when measured at the same scan rate (**Figure 5.A.9**). The sharp peaks are interpreted as free water on the surface of the paint films [13], [14]. Despite efforts to dry the surface of the films prior to measurements, these peaks were difficult to avoid when measuring thin films and featured in thermograms irreproducibly. Free water undergoes a melting transition at 0 °C, which corresponds to the second of the two melting peaks for ZnO-LO. The very low freezing transition at -43 °C is interpretated as the crystallisation of confined water [48], [49]. The melting transition of this confined water corresponds to the first melting peak in the thermograms of ZnO-LO, with an onset well below 0 °C. The freezing peak at approximately -43 °C in ZnO-LO paint films was highly reproducible (**Table 5.A.2**). The exact position, however, varied with several degrees depending on the scan rate (**Table 5.A.3**). Despite a lower water content, the same freezing/melting behaviour was observed in the thermogram of TiO_2-LO: a freezing peak at -44 °C, irregular freezing peaks between -20 and -30 °C and split melting peaks below and at 0 °C. The non-pigmented Zn-ionomer did not exhibit any freezing/melting transitions, while it did absorb water at a similar concentration as ZnO-LO at 95% RH (**Figure 5.A.1**).

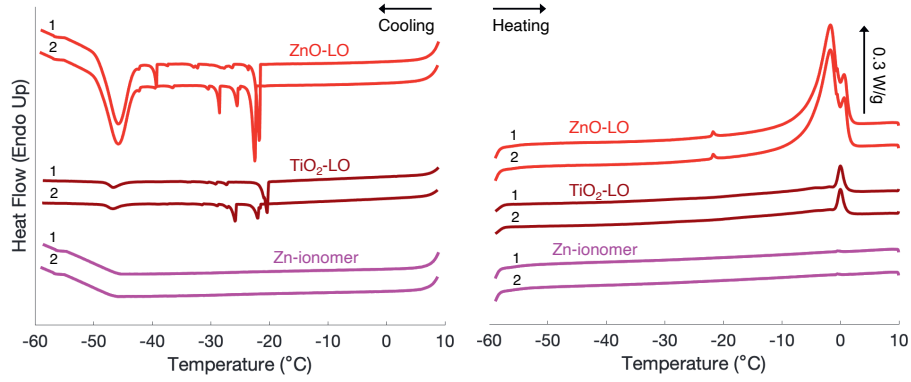

Figure 5.2 Mass-corrected DSC thermograms of water-saturated ZnO-LO, TiO_2-LO and Zn-ionomer films. Two heating and cooling cycles between 10 and -60 °C were performed with a scan rate of 5 °C/min. The numbers 1 and 2 refer to the first and second DSC run. The full DSC thermograms are reported in **Appendix 5.A**.

Cryo-FTIR spectroscopy on water-saturated paint films

The phase transitions that were observed with DSC could be confirmed with cryo-FTIR spectroscopy on thin films of the paint systems (approximately 30 µm thick) soaked in 10-30% HDO in H_2O. Moreover, the appearance of sharp OD bands at 2430 cm^{-1} (**Figure 5.3**) confirmed that the detected transitions are indeed corresponding to ice formation and melting [47]. The position of the ν_s(OD) band maximum as a function of temperature is shown in **Figure 5.4**. In ZnO-LO, there was a water freezing transition at -43 °C and a melting transition at -5 °C (**Figure 5.4a**). The TiO_2-LO profile in **Figure 5.4b** indicates a two-step transition, with the first step at -12 °C and the second at -42 °C. These transitions correspond to the freezing of two types of water as seen in the DSC thermograms: free water at -12 °C and confined water at -42 °C. ν_s(OD) shifted back to high wavenumbers at 2 °C. Due to limitations in temperature resolution, separate melting transitions for confined and bulk water could not be resolved with cryo-FTIR spectroscopy. The Zn-ionomer profile in **Figure 5.4c** did not exhibit any phase transitions.

There are interesting differences in shape and position of the OD stretch vibration band between the three paint systems. It is important to note that the OD band contains a contribution of deuterated alcohol groups that are part of the oil polymer network. The alcohol content can be estimated by comparing the OH stretch vibration band area in dried films (assumed to correspond to alcohol OH stretch vibrations only) and in H_2O-saturated films. Using this approach, the alcohol contribution was estimated to form 18%, 56% and 20% of the total OD absorbance for ZnO-LO, TiO_2-LO and Zn-ionomer, respectively (**Figure 5.A.11**). For this reason, it is not possible to analyse the OD band shape in great detail, but some additional observations can still be made. In both ZnO-LO and TiO_2-LO, a second band at 2230 cm^{-1} appeared during cooling, which is assigned to the second overtone of a librational mode ($3\nu_L$) of H_2O ice (I_h) [50], [51]. Furthermore, **Figure 5.4** clearly shows that all three profiles exhibit a redshifting trend in ν_s(OD) with decreasing temperature [45].

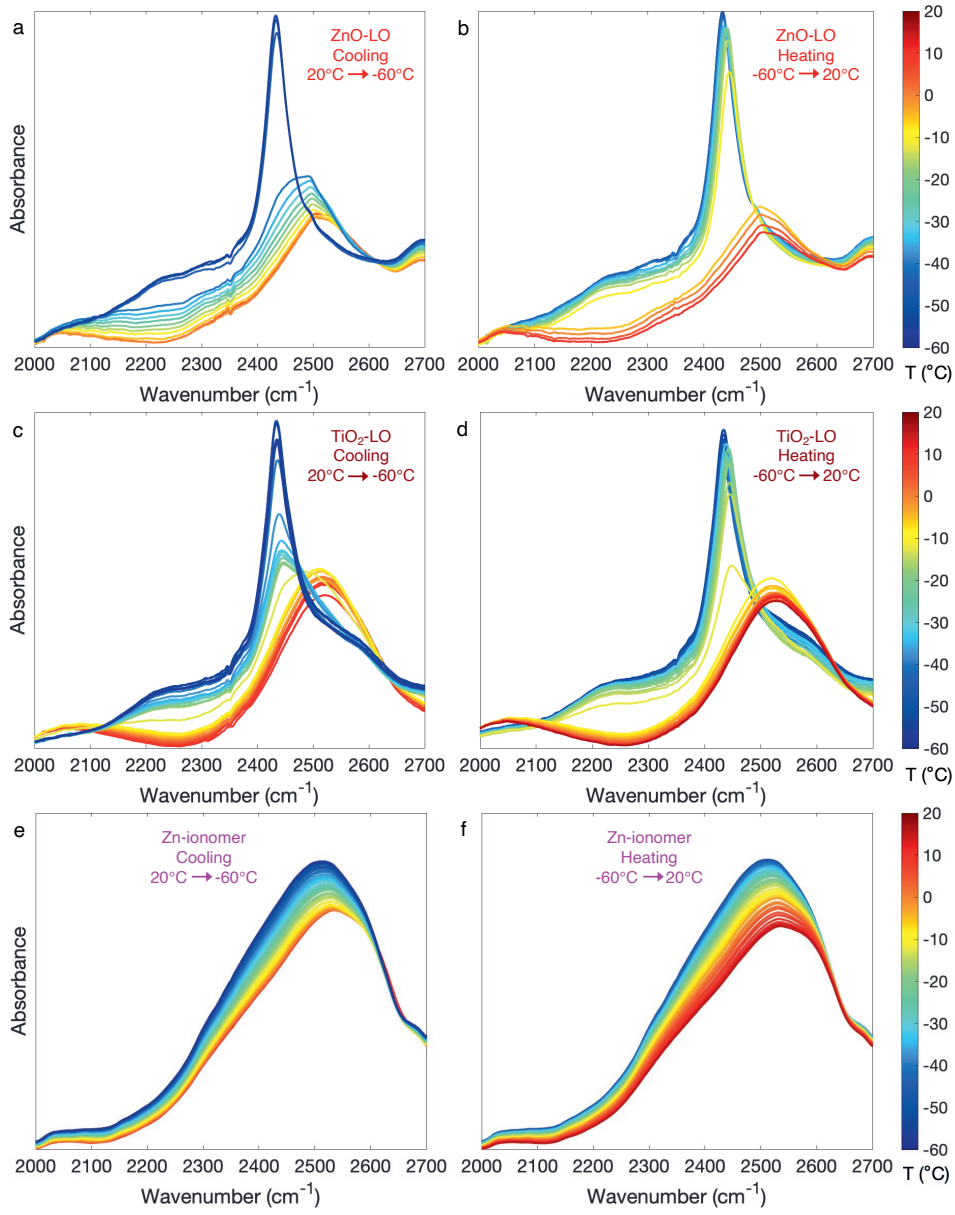

Figure 5.3 O-D stretch vibration region of the transmission FTIR spectrum of water-saturated ZnO-LO (a,b) and TiO_2-LO (c,d) (10% D_2O in H_2O) and Zn-ionomer (e,f) (30% D_2O in H_2O) during cooling and heating. The curve colours correspond to the temperature of the sample. Linear baseline subtraction was performed between 1900-4000 cm^{-1} and spectra were normalised on ν_s (CH) CH_2 at 2854 cm^{-1}.

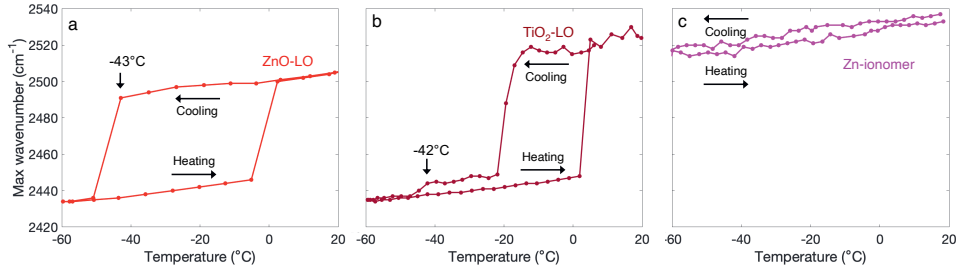

Figure 5.4 O-D vibration band maximum profiles of water-saturated ZnO-LO (red), TiO_2-LO (dark red) and Zn-ionomer (magenta). The scanning rate was 5 °C/min.

The environment of freezable water in oil paint

We observed that pigmented ZnO-LO and TiO_2-LO paints contain freezable water that underwent a freezing transition around -45 °C, whereas the non-pigmented system that models the binding medium of zinc white paint, Zn-ionomer, only contains water that did not freeze above -60 °C. These observations indicate that there are two types of water inside zinc white oil paint: non-freezable water in the binding medium and freezable clustered water located near the pigment-oil interface. The hypothesised void where this clustered water could reside between the pigment particle surface and the oil polymer network can be compared to the concept of interphase in the field of nanocomposite materials [52]. Furthermore, water accumulation at the surface of pigment particles in coatings is discussed regularly in literature as it negatively impacts the low water permeability properties of barrier coatings [7], [11].

The remarkably low freezing point of water in our systems provides interesting additional clues about the nature and environment of water clusters in oil paint. Firstly, the strong degree of supercooling is proof that the clustering water is forming discrete droplets, as opposed to a connected network of water channels. Only in small discrete volumes the probability of ice nucleation will be low enough to reach this degree of supercooling [13]. Furthermore, recent work by Hakimian et al. showed that soft confinement is a critical factor for supercooling of water to such low temperatures [53]. They were able to cool down water in octane oil to -42 °C in pores with a 2-4 nm diameter, whereas water directly in contact with the anodized aluminium oxide membrane pore wall did not supercool below -8 °C. These observations suggest that the confined water in pigmented oil paint is not just adsorbed in pores or cracks inside pigment particles, but still in at least partial contact with the oil polymer network.

A curious observation in our systems is the large hysteresis between the freezing and melting point of water. While some degree of hysteresis due to the kinetics of nucleation is expected, the hysteresis observed here for ZnO-LO is much larger compared to hysteresis generally reported for water confined in mesoporous silica gel [54]. A very interesting comparison to our systems is provided by studies on butyl rubber. A similarly large hysteresis between the freezing temperature (T_f = -38 °C) and melting temperature (T_m = -6.5 °C) of water inside butyl rubber was found, similar to our paint systems (T_f = -43 °C and T_m = -5 °C for ZnO-LO) [13]. According to Neffati et al., the large hysteresis is due to swelling of the elastic matrix of the rubber [12], [13]. Linseed oil paint films are also known to experience swelling in water (5%), although this swelling is relatively minor compared to other solvents [55]. Moreover, water inside rubber was found to disperse as droplets around hydrophilic sites [12], [13], [14]. In fact,

the investigated rubbers in the studies by Neffati et al. contained zinc oxide particles (5 wt%), which were suggested to act as hydrophilic sites where the water droplets form [13], [14].

Water cluster size estimate

It is insightful to estimate the size of water clusters in oil paint by comparison to similar confined-water systems in literature. A first estimate of the water cluster size can be made based on the confinement-induced melting point depression of ZnO-LO. The melting point is determined only by thermodynamics, as opposed to the freezing point which is also influenced by kinetics of nucleation [56]. Melting point depression can also be affected by dissolved ions or small organic molecules. Melting point depressions of several tens of Kelvins are reported for high salt concentrations (multiple M) [57], and lower concentrations of NaCl (up to 0.2 M) in mesoporous confinement may lead to melting point depressions of 20% on top of confinement-related depression [58]. If we assume that confinement is the major factor affecting the melting point of water in our systems, it is possible to calculate the radius of a spherical crystal that is surrounded by its own liquid during melting following the Gibbs-Thomson equation:

(1)

$$x = \frac{2\sigma_{\mathrm{sl}} T_{\mathrm{m}}^{\infty}}{\Delta H_{\mathrm{m}} \rho_{\mathrm{s}} \Delta T_{\mathrm{m}}}$$

Here, x is the radius of a spherical crystal, σ_{sl} corresponds to the ice-water interfacial energy, T_{m}^{∞} to the melting temperature of bulk water, ΔH_{m} to the latent heat of fusion of ice, ρ_{s} the density of ice and ΔT_{m} to the melting point depression [59]. The latent heat of fusion decreases with decreasing melting temperature [60]. As the melting temperature here is only shifted 5 K it is acceptable to use the latent heat of fusion at 273 K. These assumptions lead to a water cluster diameter $2x$ of approximately 16 nm (σ_{sl} = 22.8 ·10^{-3} Jm^2, $\Delta H_{\mathrm{m}}\rho_{\mathrm{s}}$ = 3.06 ·10^8 J/m^3 and ΔT_{m} = 5 K).

Estimating the size of water clusters is challenging in a complex environment such as oil paint. Therefore, in order to provide a reasonable range of cluster sizes we discuss two methods here. In addition to the thermodynamic approach stated above, we discuss a kinetic approach as well. Focusing on the freezing transition, several studies have discussed the relationship between freezing point depression and water cluster size. Neffati et al. based their size estimate of water clusters inside butyl rubber on the thermoporosimetry method by Brun [13], [61], [62]. They found that a freezing point of -38 °C corresponds to a cluster diameter of 3.4 nm, which they confirmed using ^{2}H-NMR relaxometry [13]. Using the same method, the water cluster diameter in ZnO-LO would be approximately 3 nm. Pelster et al. reported a freezing temperature of water in butyl rubber of -43 °C and an experimentally determined cluster diameter of 2.6 nm based on thermally stimulated depolarisation current (TSDC) and small-angle X-ray scattering (SAXS) analysis, while Spehr et al. reported a supercooling of 50 °C for reverse micelles with a diameter just below 2 nm [63]. Using a different approach, Dokter et al. showed that the IR spectral features of ice in reverse micelles are dependent on the number of water molecules inside the micelle. Water in reverse micelles containing fewer than 200 molecules forms amorphous ice with a broad spectral feature around 2500 cm^{-1}, whereas groups of over 200 water molecules form crystalline ice with a sharp band at 2435 cm^{-1}. Based on the presence of the sharp O-D band at 2435 cm^{-1} in the cryo-FTIR spectrum of ZnO-LO, we can infer a minimum cluster size of 200 water molecules [46], which correspond to a

spherical volume with a diameter of 2.24 nm based on the molar volume of water. This conclusion is in line with the observation that water crystallisation inside mesoporous silica gel with a pore diameter of 2.1 nm was inhibited [64].

Combining all the evidence, based on the melting and freezing points of water in ZnO-LO, we estimate the diameter of the water clusters in this oil paint between 2 nm and 16 nm. If the confined water clusters in ZnO-LO are indeed of nanometre size, we should expect to see evidence of this confinement in the FTIR spectra. The ν_s(OD) band is known to shift to higher frequency with a decreasing size of confined water clusters [65], [66]. A blueshift for reverse micelles is reported from 2512 cm^{-1} for bulk water to 2565 cm^{-1} for interfacial water, which is water that interacts directly with micelle boundary [65]. ν_s(OD) at room temperature for ZnO-LO is located at 2505 cm^{-1}, very similar to that of bulk water [47]. This band positions suggests that a large fraction of the water in ZnO-LO is bulk-like liquid water, and that the size is likely to be at the high end of our 2-16 nm estimate. Conversely, in the case of Zn-ionomer, it seems likely that the cluster size is below the 200-molecule limit, as both DSC and cryo-FTIR analysis indicate that the water present inside the Zn-ionomer does not undergo a freezing transition above -60 °C. Data reported by Spehr et al. suggests that a freezing point below -60 °C would correspond to a very small cluster radius of only a few Å [63]. A smaller water cluster size in Zn-ionomer compared to ZnO-LO is also supported by the strong blueshift of ν_s(OD) for Zn-ionomer (2534 cm^{-1}) compared to ZnO-LO (2502 cm^{-1}). This blueshift in Zn-ionomer indicates that Zn-ionomer contains a larger contribution of interfacial water. For these reasons, we classify the water in Zn-ionomer as non-freezable and molecularly distributed.

Implications of water clusters on chemical reactivity and paintings conservation

Our experiments indicate that water in zinc white oil paint is heterogeneously distributed as molecularly dispersed water in the oil polymer network and liquid-like water near the pigment-polymer interface. In addition, we see evidence that the presence of zinc ions in the polymer network positively influences the water sorption capacity of the polymer, given the low water sorption in titanium white paint. This conclusion is supported by studies on polyethylene zinc ionomer systems, where the presence of zinc ions increased the water sorption capacity [67], [68]. These findings have large implications for our understanding of chemical change in oil paint pigmented with zinc white or other pigments. We imagine that liquid-like water located near the zinc oxide surface can stabilise and/or dissolve ions and small polar molecules. As such, water clusters could accelerate reactions between pigments and carboxylic acid groups or other functionalities that break down the pigment or facilitate recrystallisation of pigments to new mineral phases [20], [69], [70], [71], [72], [73], [74], [75], [76]. In addition, ionic species could diffuse through regions of the paint in solvated form when liquid water is present, while this diffusion is likely to be much slower in the absence of liquid water.

A crucial step towards understanding the practical implications of these findings in a conservation context is to know which environmental conditions lead to water cluster formation in oil paint. The measurements in this work were performed on water-saturated paint films. It is important to know whether clustered water may form in oil paints in a typical museum climate, where humidity from the air is the primary source of moisture. For that goal, we performed DSC measurements on ZnO-LO conditioned at 90% relative humidity (**Figure 5.A.10**). No water freezing/melting transitions were detected under those conditions. This result suggests that water clusters only arise in (near-) saturated conditions. These conditions could arise in the surface region of paint during liquid water exposure, for instance during

cleaning and consolidation interventions using aqueous solutions. Generally, conservators take utmost care to control water exposure during these types of interventions, for example by using gels or tissues to deliver a solution to a painted surface.

A further important question is whether the clustering of water in water-saturated paints also occurs in paints with different pigmentation. Preliminary DSC experiments were performed according to the method described above on pigmented linseed oil paint films with red lead (minium, Pb_3O_4), carbon black (C) and iron oxide (Fe_2O_3). In addition, a lead ionomer model system was tested. The preparation of the paint films is discussed in **Appendix 5.B**. It was found that all paint films containing pigments exhibited freezing and melting peaks associated with clustered water (**Figures 5.B.1-3**). The lead-ionomer model system did not exhibit any peaks (**Figure 5.B.4**). These results indicate that the phenomenon of clustering water near the pigment-oil interface in water-saturated films is not limited to ZnO-LO and TiO_2-LO but more widespread. Further research on this topic will be necessary to understand how widespread this phenomenon is, and which pigment properties favour the formation of clustered water in oil paints.

In addition, quantification of the ratio freezable to nonfreezable water would provide additional insights into the behaviour of water in oil paint. Essential for calculating the ratio between the two states of water is a reliable measure of the total moisture content in the water-saturated paint films. A first attempt at calculating the ratio was done, discussed in more detail in **Appendix 5.B**. The total water content in water-saturated iron oxide-LO, carbon black-LO and ZnO-LO was determined gravimetrically in triplicate. Integration of the melting peak associated with clustered water allowed the calculation of the content of freezable water and the weight fraction freezable water to total water content (**Figure 5.B.5**). For iron oxide-LO, carbon black-LO and ZnO-LO, the weight fraction of freezable water to the total water content was found to be 0.04, 0.07 and 0.11 respectively (**Table 5.B.2**). These results indicate that the vast majority of water inside a water-saturated oil paint is located in the binding medium, molecularly dispersed or in clusters small enough to be nonfreezable. Only a small fraction of the water forms clusters of freezable water. Once a robust method for the quantification of the ratio freezable to nonfreezable water is established, paint films with varying pigment concentrations or particle size can be investigated, which could lead to valuable additional insights in the distribution of water in pigmented paint films.

Lastly, our future research will focus on investigating the rate and location of clustered water formation in oil paint during treatment. In an effort to provide conservators with tools to guide decision-making around treating sensitive oil paint, it would be interesting to explore non-invasive techniques for monitoring of water-based conservation treatments.

5.4 Conclusions

In this work a complimentary combination of DSC and cryo-FTIR spectroscopy was used successfully to detect heterogeneity in water distribution in oil paint at the nanoscale. We have shown that zinc white oil paint contains molecularly dispersed water in the polymerised oil binder and liquid-like water clusters with nanometre size near the pigment-polymer interface under saturated conditions. The presence of liquid-like water clusters has important implications for our understanding of chemical processes in oil paint. These findings change

our perspective on oil paint chemistry as they prompt us to consider aqueous chemistry when studying paint degradation. Furthermore, the results lead to a wide range of new questions, both fundamental and practical. Future research will focus on extending the research to oil paints with different pigments and degrees of ageing. Moreover, non-invasive monitoring techniques may be used to establish object-specific guidelines. Finally, investigations into the effect of clustered water on pigment-binder reactions will help establishing the important link between water exposure and reactivity in paintings, which is critical information for establishing safe parameters for storage, display, and treatment of painted works of art.

5.5 Acknowledgements

This research was supported by The Bennink Foundation/Rijksmuseum Fonds. Joen Hermans was supported by the Netherlands Organization for Scientific Research (NWO) under project number 016.Veni.192.052. Federico Caporaletti was Chargé de Research of the Fonds de la Recherche Scientifique – FNRS. The authors are grateful to Bas de Bruin and Felix de Zwart for supporting the DSC measurements. Francesca Gabrieli and Piet Iedema are thanked for useful discussions. Stefano Renzetti is acknowledged for his support with the DVS analysis.

5.6 References

[1] M.-C. Bellissent-Funel, 'Hydrophilic–hydrophobic interplay: from model systems to living systems', *Comptes Rendus Geoscience*, vol. 337, no. 1, pp. 173–179, 2005.

[2] C. Cuadrado-Collados, A. A. Majid, M. Martinez-Escandell, L. L. Daemen, A. Missyul, C. Koh, and J. Silvestre-Albero, 'Freezing/melting of water in the confined nanospace of carbon materials: Effect of an external stimulus', *Carbon*, vol. 158, pp. 346–355, 2020.

[3] P. Kreider, A. Cardew-Hall, S. Sommacal, A. Chadwick, S. Hümbert, S. Nowotny, D. Nisbet, A. Tricoli, and P. Compston, 'The effect of a superhydrophobic coating on moisture absorption and tensile strength of 3D-printed carbon-fibre/polyamide', *Composites Part A: Applied Science and Manufacturing*, vol. 145, art. 106380, 2021.

[4] M. Shaat and Y. Zheng, 'Fluidity and phase transitions of water in hydrophobic and hydrophilic nanotubes', *Scientific Reports*, vol. 9, no. 1, art. 5689, 2019.

[5] K. T. Tan, S. Tao, N. Huang, and D. Jiang, 'ater cluster in hydrophobic crystalline porous covalent organic frameworks', *Nature Communications*, vol. 12, no. 1, art. 6747, 2021.

[6] I. Martín-Fabiani, J. Lesage de la Haye, M. Schulz, Y. Liu, M. Lee, B. Duffy, F. D'Agosto, M. Lansalot, and J. L. Keddie, 'Enhanced water barrier properties of surfactant-free polymer films obtained by MacroRaFT-mediated emulsion polymerization', *ACS Applied Materials & Interfaces*, vol. 10, no. 13, pp. 11221–11232, 2018.

[7] G. Van der Wel and O. Adan, 'Moisture in organic coatings—a review', *Progress in Organic Coatings*, vol. 37, no. 1, pp. 1–14, 1999.

[8] C. Yang, X. Xing, Z. Li, and S. Zhang, 'A comprehensive review on water diffusion in polymers focusing on the polymer–metal interface combination', *Polymers*, vol. 12, no. 1, art. 138, 2020.

[9] H. Zargarnezhad, E. Asselin, D. Wong, and C. C. Lam, 'A critical review of the time-dependent performance of polymeric pipeline coatings: Focus on hydration of epoxy-based coatings', *Polymers*, vol. 13, no. 9, art. 1517, 2021.

[10] B. H. Zimm and J. L. Lundberg, 'Sorption of vapors by high polymers', *The Journal of Physical Chemistry*, vol. 60, no. 4, pp. 425–428, 1956.

[11] S. Morsch, S. Lyon, P. Greensmith, S. Smith, and S. Gibbon, 'Mapping water uptake in organic coatings using AFM-IR', *Faraday Discussions*, vol. 180, pp. 527–542, 2015.

[12] A. Thomas and K. Muniandy, 'Absorption and desorption of water in rubbers', *Polymer*, vol. 28, no. 3, pp. 408–415, 1987.

[13] R. Neffati, P. Judeinstein, and J. Rault, 'Supercooled nano-droplets of water confined in hydrophobic rubber', *Physical Chemistry Chemical Physics*, vol. 23, no. 44, pp. 25347–25355, 2021.

[14] R. Pelster, A. Kops, G. Nimtz, A. Enders, H. Kietzmann, P. Pissis, A. Kyritsis, and Woermann, 'On mesoscopic water droplets dispersed in butyl rubber', *Berichte der Bunsengesellschaft für physikalische Chemie*, vol. 97, no. 5, pp. 666–675, 1993.

[15] Y. Taniguchi, K. Kawahara, M. Takashima, M. Cotte, J. Mazurek, Y. Kumazawa, Y. Taga, and T. Nakazawa, 'Organic Materials Used for Giant Buddhas and Wall Paintings in Bamiyan, Afghanistan', *Applied Sciences*, vol. 12, no. 19, art. 9476, 2022.

[16] Y. Orlova, R. E. Harmon, L. J. Broadbelt, and P. D. Iedema, 'Review of the kinetics and simulations of linseed oil autoxidation', *Progress in Organic Coatings*, vol. 51, art. 106041, 2021.

[17] L. Baij, L. Chassouant, J. J. Hermans, K. Keune, and P. D. Iedema, 'The concentration and origins of carboxylic acid groups in oil paint', *RSC Advances*, vol. 9, no. 61, pp. 35559–35564, 2019.

[18] L. De Viguerie, P. Payard, E. Portero, P. Walter, and M. Cotte, 'The drying of linseed oil investigated by Fourier transform infrared spectroscopy: Historical recipes and influence of lead compounds', *Progress in Organic Coatings*, vol. 93, pp. 46–60, 2016.

[19] S. Garrappa, E. Kočí, S. Švarcová, P. Bezdička, and D. Hradil, 'Initial stages of metal soapsformation in model paints: The role of humidity', *Microchemical Journal*, vol. 156, art. 104842, 2020.

[20] J. J. Hermans, K. Keune, A. Van Loon, and P. D. Iedema, 'Toward a complete molecular model for the formation of metal soaps in oil paints', in *Metal Soaps in Art*, F. Casadio, K. Keune, P. Noble, A. van Loon, E. Hendriks, S. A. Centeno, and G. Osmond, Eds., Cham: Springer, 2019, pp. 47–67.

[21] R. J. Meilunas, J. G. Bentsen, and A. Steinberg, 'Analysis of aged paint binders by FTIR spectroscopy', *Studies in Conservation*, vol. 35, no. 1, pp. 33–51, 1990.

[22] L. H. Oakley, F. Casadio, P. K. R. Shull, and P. L. J. Broadbelt, 'Modeling the Evolution of Crosslinked and Extractable Material in an Oil-Based Paint Model System', *Angewandte Chemie International Edition*, vol. 57, no. 25, pp. 7413–7417, 2018.

[23] K. Sutherland, 'Solvent-extractable components of linseed oil paint films', *Studies in Conservation*, vol. 48, no. 2, pp. 111–135, 2003.

[24] C. Krarup Andersen, A. Freeman, M. N. Mortensen, V. Beltran, M. Łukomski, and A. Phenix, 'Mechanical and Moisture Sorption Properties of Commercial Artists' Oil Paint by Dynamic Mechanical Thermal Analysis (DMA), Nanoindentation, and Dynamic Vapour Sorption (DVS)', in *Conservation of Modern Oil Paintings*, K. J. van den Berg, I. Bonaduce, A. Burnstock, B. Ormsby, M. Scharff, L. Carlyle, G. Heydenreich, and K. Keune, Eds., Cham: Springer, 2019, pp. 403–418.

[25] L. Baij, J. J. Hermans, K. Keune, and P. Iedema, 'Time-Dependent ATR-FTIR Spectroscopic Studies on Fatty Acid Diffusion and the Formation of Metal Soaps in Oil Paint Model Systems', *Angewandte Chemie International Edition*, vol. 57, no. 25, pp. 7351–7354, 2018.

[26] T. Chan and M. Odlyha, 'The effect of relative humidity and pigment type on paint films', *Thermochimica Acta*, vol. 269, pp. 755–767, 1995.

[27] J. R. Duivenvoorden, R. P. Kramer, M. H. van Eikema Hommes, P. D. Iedema, J. J. Hermans, and K. Keune, 'The distribution and transport of water in oil paintings: A numerical moisture diffusion model', *International Journal of Heat and Mass Transfer*, vol. 202, art. 123682, 2023.

[28] R. MacBeth, 'The Moisture Sorption of Eleven Oil Paint Samples', Master's Thesis, The Courtauld Institute of Art, 1988.

[29] L. E. Raven, M. Bisschoff, M. Leeuwestein, M. Geldof, J. J. Hermans, M. Stols-Witlox, and K. Keune, 'Delamination due to zinc soap formation in an oil painting by Piet Mondrian (1872–1944)', in *Metal Soaps in Art*, F. Casadio, K. Keune, P. Noble, A. van Loon, E. Hendriks, S. A. Centeno, and G. Osmond, Eds., Cham: Springer, 2019, pp. 343–358.

[30] F. Gabrieli, F. Rosi, A. Vichi, L. Cartechini, L. Pensabene Buemi, S. G. Kazarian, and C. Miliani, 'Revealing the nature and distribution of metal carboxylates in Jackson Pollock's Alchemy (1947) by micro-attenuated total reflection FT-IR spectroscopic imaging', *Analytical Chemistry*, vol. 89, no. 2, pp. 1283–1289, 2017.

[31] F. Casadio and V. Rose, 'High-resolution fluorescence mapping of impurities in historical zinc oxide pigments: hard X-ray nanoprobe applications to the paints of Pablo Picasso', *Applied Physics A*, vol. 111, pp. 1–8, 2013.
[32] G. Osmond, 'Zinc soaps: an overview of zinc oxide reactivity and consequences of soap formation in oil-based paintings', in *Metal Soaps in Art*, F. Casadio, K. Keune, P. Noble, A. van Loon, E. Hendriks, S. A. Centeno, and G. Osmond, Eds., Cham: Springer, 2019, pp. 25–46.
[33] J. J. Hermans, K. Keune, A. van Loon, R. W. Corkery, and P. D. Iedema, 'Ionomer-like structure in mature oil paint binding media', *RSC Advances*, vol. 6, no. 96, pp. 93363–93369, 2016.
[34] M. Beerse, K. Keune, P. D. Iedema, S. Woutersen, and J. J. Hermans, 'The Evolution of Zinc Carboxylate Species in Oil Paint Ionomers', *ACS Applied Polymer Materials*, vol. 2, pp. 5674−5685, 2020.
[35] J. J. Hermans, L. Baij, M. Koenis, K. Keune, P. D. Iedema, and S. Woutersen, '2D-IR spectroscopy for oil paint conservation: Elucidating the water-sensitive structure of zinc carboxylate clusters in ionomers', *Science Advances*, vol. 5, no. 6, art. eaaw3592, 2019.
[36] J. J. Hermans, K. Helwig, S. Woutersen, and K. Keune, 'Traces of water catalyze zinc soap crystallization in solvent-exposed oil paint', *Physical Chemistry Chemical Physics*, vol. 25, no. 7, pp. 5701–5709, 2023.
[37] V. Di Tullio, N. Zumbulyadis, S. Centeno, J. Catalano, M. Wagner, and C. Dybowski, 'Water Diffusion and Transport in Oil Paints as Studied by Unilateral NMR and 1H High-Resolution MAS-NMR Spectroscopy', *ChemPhysChem*, vol. 21, no. 1, pp. 113–119, 2020.
[38] S. M. Dron and M. Paulis, 'Tracking Hydroplasticization by DSC: Movement of Water Domains Bound to Poly (Meth) Acrylates during Latex Film Formation', *Polymers*, vol. 12, no. 11, art. 2500, 2020.
[39] D. Faroongsarng and P. Sukonrat, 'Thermal behavior of water in the selected starch-and cellulose-based polymeric hydrogels', *International Journal of Pharmaceutics*, vol. 352, no. 1, pp. 152–158, 2008.
[40] P. Geng, A. Zore, and M. R. Van De Mark, 'Thermodynamic characterization of free and surface water of colloidal unimolecular polymer (CUP) particles utilizing DSC', *Polymers*, vol. 12, no. 6, art. 1417, 2020.
[41] T. Nakano and T. Nakaoki, 'Coagulation size of freezable water in poly (vinyl alcohol) hydrogels formed by different freeze/thaw cycle periods', *Polymer Journal*, vol. 43, no. 11, pp. 875–880, 2011.
[42] Z. Ping, Q. Nguyen, S. Chen, J. Zhou, and Y. Ding, 'States of water in different hydrophilic polymers—DSC and FTIR studies', *Polymer*, vol. 42, no. 20, pp. 8461–8467, 2001.
[43] P. Talik and U. Hubicka, 'The DSC approach to study non-freezing water contents of hydrated hydroxypropylcellulose (HPC)', *Journal of Thermal Analysis and Calorimetry*, vol. 132, no. 1, pp. 445–451, 2018.
[44] F. Rull, 'Structural investigation of water and aqueous solutions by Raman spectroscopy', *Pure and Applied Chemistry*, vol. 74, no. 10, pp. 1859–1870, 2002.
[45] F. Caporaletti, D. Bonn, and S. Woutersen, 'Lifetime-Associated Two-Dimensional Infrared Spectroscopy Reveals the Hydrogen-Bond Structure of Supercooled Water in Soft Confinement', *The Journal of Physical Chemistry Letters*, vol. 12, no. 25, pp. 5951–5956, 2021.

[46] A. M. Dokter, C. Petersen, S. Woutersen, and H. J. Bakker, 'Vibrational dynamics of ice in reverse micelles', *The Journal of Chemical Physics*, vol. 128, no. 4, art. 044509, 2008.
[47] J. R. Scherer and R. G. Snyder, 'Raman intensities of single crystal ice I_h', *The Journal of Chemical Physics*, vol. 67, no. 11, pp. 4794–4811, 1977.
[48] Y. P. Handa, M. Zakrzewski, and C. Fairbridge, 'Effect of restricted geometries on the structure and thermodynamic properties of ice', *The Journal of Physical Chemistry*, vol. 96, no. 21, pp. 8594–8599, 1992.
[49] J. B. W. Webber, 'Studies of nano-structured liquids in confined geometry and at surfaces', *Progress in Nuclear Magnetic Resonance Spectroscopy*, vol. 56, no. 1, pp. 78–93, 2017.
[50] D. Hornig, H. White, and F. Reding, 'The infrared spectra of crystalline H_2O, D_2O and HDO', *Spectrochimica Acta*, vol. 12, no. 4, pp. 338–349, 1958.
[51] W. Hagen, A. Tielens, and J. Greenberg, 'The infrared spectra of amorphous solid water and ice I_c between 10 and 140 K', *Chemical Physics*, vol. 56, no. 3, pp. 367–379, 1981.
[52] D. Ciprari, K. Jacob, and R. Tannenbaum, 'Characterization of polymer nanocomposite interphase and its impact on mechanical properties', *Macromolecules*, vol. 39, no. 19, pp. 6565–6573, 2006.
[53] A. Hakimian, M. Mohebinia, M. Nazari, A. Davoodabadi, S. Nazifi, Z. Huang, J. Bao, and H. Ghasemi, 'Freezing of few nanometers water droplets', *Nature Communications*, vol. 12, no. 1, art. 6973, 2021.
[54] K. Morishige and K. Kawano, 'Freezing and melting of water in a single cylindrical pore: The pore-size dependence of freezing and melting behavior', *The Journal of Chemical Physics*, vol. 110, no. 10, pp. 4867–4872, 1999.
[55] L. Baij, J. J. Hermans, K. Keune, and P. D. Iedema, 'Time-dependent ATR-FTIR spectroscopic studies on solvent diffusion and film swelling in oil paint model systems', *Macromolecules*, vol. 51, no. 18, pp. 7134–7144, 2018.
[56] R. A. Jones, *Soft Condensed Matter*, vol. 6. Oxford: Oxford University Press, 2002.
[57] C. P. Lamas, C. Vega, and E. G. Noya, 'Freezing point depression of salt aqueous solutions using the Madrid-2019 model', *The Journal of Chemical Physics*, vol. 156, no. 13, art. 134503, 2022.
[58] C. M. Burba and J. Janzen, 'Confinement effects on the phase transition temperature of aqueous NaCl solutions: The extended Gibbs–Thomson equation', *Thermochimica Acta*, vol. 615, pp. 81–87, 2015.
[59] J. Mitchell, J. B. W. Webber, and J. H. Strange, 'Nuclear magnetic resonance cryoporometry', *Physics Reports*, vol. 461, no. 1, pp. 1–36, 2008.
[60] R. Neffati, P. Judeinstein, and J. Rault, 'Freezing, melting and dynamics of supercooled water confined in porous glass', *Journal of Physics: Condensed Matter*, vol. 32, no. 46, art. 465101, 2020.
[61] R. Neffati, L. Apekis, and J. Rault, 'Size distribution of water droplets in butyl rubber application of DSC in thermoporosimetry', *Journal of Thermal Analysis and Calorimetry*, vol. 54, pp. 741–752, 1998.
[62] M. Brun, A. Lallemand, J.-F. Quinson, and C. Eyraud, 'A new method for the simultaneous determination of the size and shape of pores: the thermoporometry', *Thermochimica Acta*, vol. 21, no. 1, pp. 59–88, 1977.
[63] T. Spehr, B. Frick, I. Grillo, and B. Stühn, 'Supercooling of water confined in reverse micelles', *Journal of Physics: Condensed Matter*, vol. 20, no. 10, art. 104204, 2008.
[64] S. Kittaka, S. Takahara, H. Matsumoto, Y. Wada, T. J. Satoh, and T. Yamaguchi, 'Low temperature phase properties of water confined in mesoporous silica MCM-41:

Thermodynamic and neutron scattering study', *The Journal of Chemical Physics*, vol. 138, no. 20, art. 204714, 2013.

[65] P. A. Pieniazek, Y.-S. Lin, J. Chowdhary, B. M. Ladanyi, and J. Skinner, 'Vibrational spectroscopy and dynamics of water confined inside reverse micelles', *The Journal of Physical Chemistry B*, vol. 113, no. 45, pp. 15017–15028, 2009.

[66] T. H. van der Loop, M. R. Panman, S. Lotze, J. Zhang, T. Vad, H. J. Bakker, W. F. Sager, and S. Woutersen, 'Structure and dynamics of water in nonionic reverse micelles: A combined time-resolved infrared and small angle x-ray scattering study', *The Journal of Chemical Physics*, vol. 137, no. 4, art. 044503, 2012.

[67] K.-I. Itoh, Y. Tsujita, A. Takizawa, and T. Kinoshita, 'Sorption and permeation behavior of water vapor and carbon dioxide gas through ethylene ionomer membranes', *Journal of Applied Polymer Science*, vol. 32, no. 1, pp. 3335–3343, 1986.

[68] R. Weiss, A. Sen, C. Willis, and L. Pottick, 'Block copolymer ionomers: 1. Synthesis and physical properties of sulphonated poly (styrene-ethylene/butylene-styrene)', *Polymer*, vol. 32, no. 10, pp. 1867–1874, 1991.

[69] F. Vanmeert, G. Van der Snickt, and K. Janssens, 'Plumbonacrite identified by X-ray powder diffraction tomography as a missing link during degradation of red lead in a Van Gogh painting', *Angewandte Chemie International Edition*, vol. 127, no. 12, pp. 3678–3681, 2015.

[70] L. Monico, K. Janssens, M. Cotte, L. Sorace, F. Vanmeert, B. G. Brunetti, and C. Miliani, 'Chromium speciation methods and infrared spectroscopy for studying the chemical reactivity of lead chromate-based pigments in oil medium', *Microchemical Journal*, vol. 124, pp. 272–282, 2016.

[71] K. Keune, J. Mass, F. Meirer, C. Pottasch, A. van Loon, A. Hull, J. Church, E. Pouyet, M. Cotte, and A. Mehta, 'Tracking the transformation and transport of arsenic sulfide pigments in paints: synchrotron-based X-ray micro-analyses', *Journal of Analytical Atomic Spectrometry*, vol. 30, no. 3, pp. 813–827, 2015.

[72] J. J. Boon, J. van der Weerd, K. Keune, P. Noble, and J. Wadum, 'Mechanical and chemical changes in Old Master paintings: dissolution, metal soap formation and remineralization processes in lead pigmented ground/intermediate paint layers of 17th century paintings', in *Preprints of the ICOM Committee for Conservation 13th Triennial Meeting, Rio de Janeiro 21-28 Sept 2002*, C. Antomarchi, Ed., London: James and James, 2002, pp. 401–406.

[73] V. Gonzalez, A. van Loon, S. W. Price, P. Noble, and K. Keune, 'Synchrotron micro-XRD and micro-XRD-CT reveal newly formed lead–sulfur compounds in Old Master paintings', *Journal of Analytical Atomic Spectrometry*, vol. 35, no. 10, pp. 2267–2273, 2020.

[74] F. Modugno, F. Di Gianvincenzo, I. Degano, I. D. van der Werf, I. Bonaduce, and K. J. van den Berg, 'On the influence of relative humidity on the oxidation and hydrolysis of fresh and aged oil paints', *Scientific Reports*, vol. 9, no. 1, pp. 1–16, 2019.

[75] O. Ranquet, C. Duce, E. Bramanti, P. Dietemann, I. Bonaduce, and N. Willenbacher, 'A holistic view on the role of egg yolk in Old Masters' oil paints', *Nature Communications*, vol. 14, no. 1, art. 1534, 2023.

[76] M. Karel, 'Lipid oxidation, secondary reactions, and water activity of foods', in *Autoxidation in Food and Biological Systems*, Cham: Springer, 1980, pp. 191–206.

5.A Appendix 1

Additional experimental details

Zinc sorbate (ZnSo) was synthesised by adding 0.559 g sorbic acid (Sigma, ≥99.0%) and 1 mL triethylamine (Sigma-Aldrich, ≥99.5%) to 20 mL deionised water at 60 °C. 1.016 g zinc nitrate hexahydrate (Sigma-Aldrich, ≥99.0%) was dissolved in 5 mL deionised water. This solution was added dropwise to the sorbic acid solution and left stirring for 20 minutes. The precipitated ZnSo was separated by vacuum filtration, washed with water and acetone before drying overnight over phosphorus pentoxide under vacuum. The zinc ionomer model systems (Zn-ionomer) were prepared by mixing 0.074 g ZnSo in 0.53 mL LO with mortar and pestle. This mixture was applied on glass slides using a drawdown bar (30 and 90 µm) and left to cure overnight in the dark at 150 °C.

Water sorption isotherms

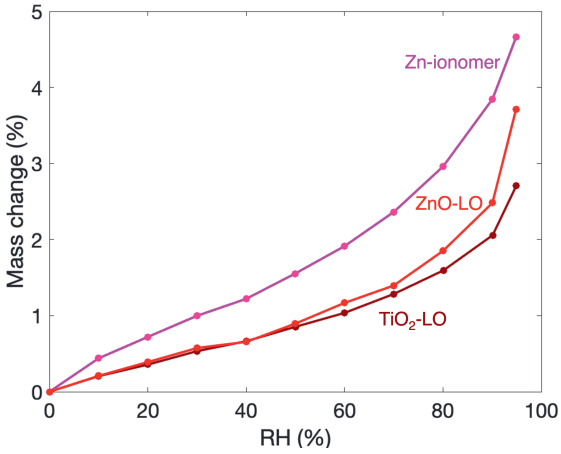

Figure 5.A.1 Water sorption isotherms showing the mass change (%) of ZnO-LO, TiO_2-LO and Zn-ionomer films as a result of exposure to humid air between 0 and 95% RH.

Melting and freezing points determined by DSC

Table 5.A.1 Melting and freezing points of ZnO-LO, TiO_2-LO and Zn-ionomer.

Sample name	ZnO-LO	TiO_2-LO	Zn-ionomer
Onset cold freezing peak (°C)			
Cycle 1	-43.1	-44.4	-
Cycle 2	-43.2	-44.3	-
Minimum cold freezing peak (°C)			
Cycle 1	-45.8	-46.6	-
Cycle 2	-45.8	-46.6	-
Onset melting peak 1 (°C)			
Cycle 1	-5.2	-6.5	-
Cycle 2	-5.2	-6.8	-
Maximum melting peak 1 (°C)			
Cycle 1	-1.7	-4.1	-
Cycle 2	-1.7	-3.8	-
Onset melting peak 2 (°C)			
Cycle 1	-2.2	-0.8	-
Cycle 2	-2.4	-0.7	-
Maximum melting peak 2 (°C)			
Cycle 1	-0.7	0.0	-
Cycle 2	-0.7	0.0	-

Table 5.A.2 Melting and freezing points of two more ZnO-LO paint films from the same batch.

Sample name	ZnO-LO-2	ZnO-LO-3
Onset cold freezing peak (°C)		
Cycle 1	-42.9	-42.6
Cycle 2	-42.9	-42.9
Minimum cold freezing peak (°C)		
Cycle 1	-45.9	-45.0
Cycle 2	-45.6	-45.7
Onset melting peak 1 (°C)		
Cycle 1	-6.0	-5.2
Cycle 2	-5.6	-5.0
Maximum melting peak 1 (°C)		
Cycle 1	-1.8	-1.2
Cycle 2	-1.8	-1.3
Onset melting peak 2 (°C)		
Cycle 1	-1.1	-2.3
Cycle 2	-1.2	-3.1
Maximum melting peak 2 (°C)		
Cycle 1	-0.3	-0.2
Cycle 2	-0.4	-0.3

Table 5.A.3 Melting and freezing points of ZnO-LO with different DSC scanning rates.

Scanning rate		5 °C/min	10 °C/min	20 °C/min
Onset cold freezing peak (°C)				
	Cycle 1	-43.2	-42.6	-45.0
	Cycle 2	-43.2	-42.6	-45.1
Minimum cold freezing peak (°C)				
	Cycle 1	-45.3	-44.5	-46.9
	Cycle 2	-45.4	-45.5	-47.0
Onset melting peak (°C)				
	Cycle 1	-4.4	-4.2	-3.3
	Cycle 2	-4.4	-4.2	-3.4
Maximum melting peak (°C)				
	Cycle 1	-1.5	-0.9	-0.3
	Cycle 2	-1.5	-0.9	-0.3

DSC thermograms

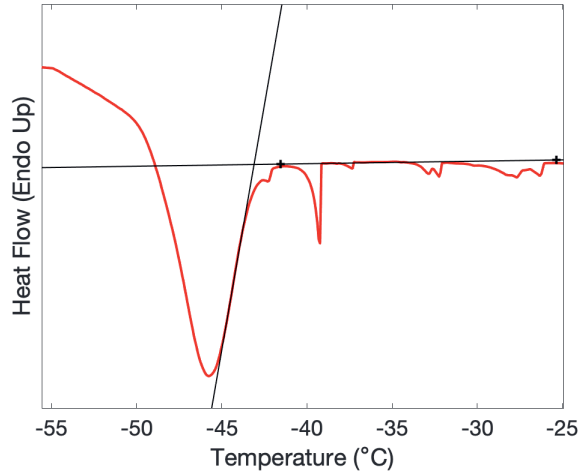

Figure 5.A.2 Example of calculation of onset of a peak. The onset is defined as the point where the tangent intersects the baseline.

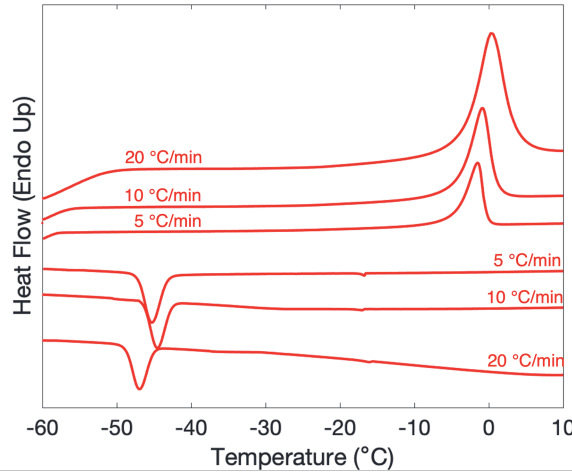

Figure 5.A.3 Freezing and melting transitions of ZnO-LO with different scanning rates.

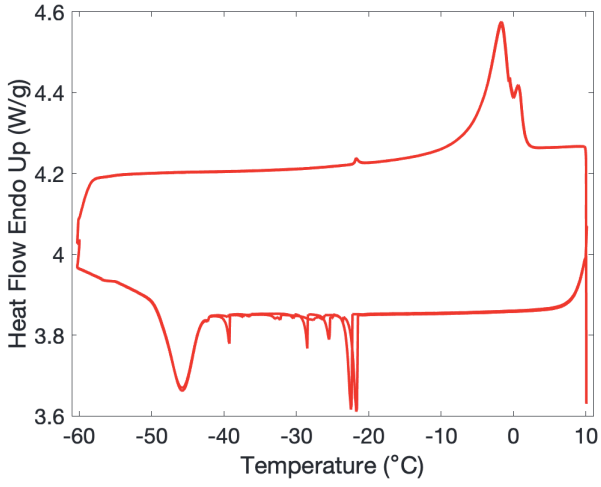

Figure 5.A.4 DSC thermogram of ZnO-LO corrected for the sample weight (5.67 mg).

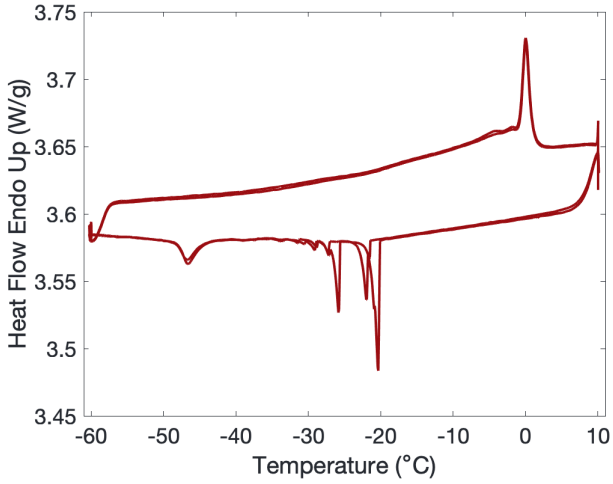

Figure 5.A.5 DSC thermogram of TiO_2-LO corrected for the sample weight (5.83 mg).

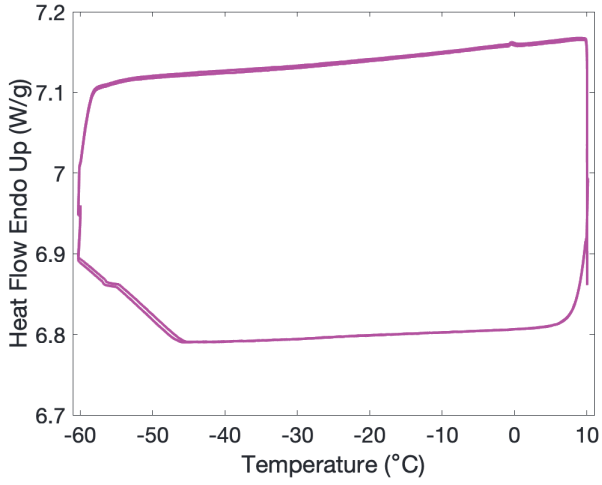

Figure 5.A.6 DSC thermogram of Zn-ionomer corrected for the sample weight (4.71 mg).

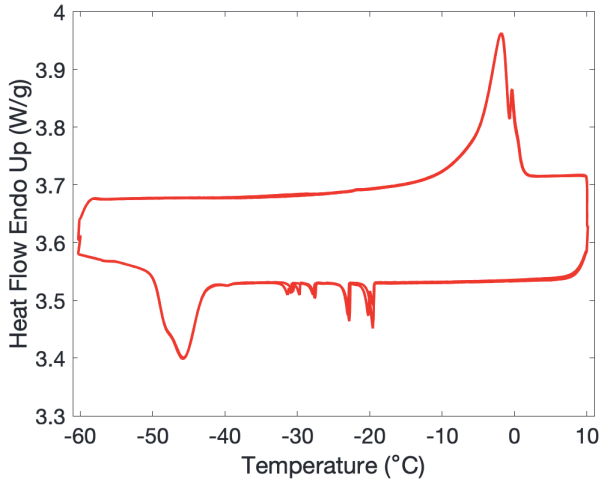

Figure 5.A.7 DSC thermogram of ZnO-LO-2 corrected for the sample weight (5.51 mg).

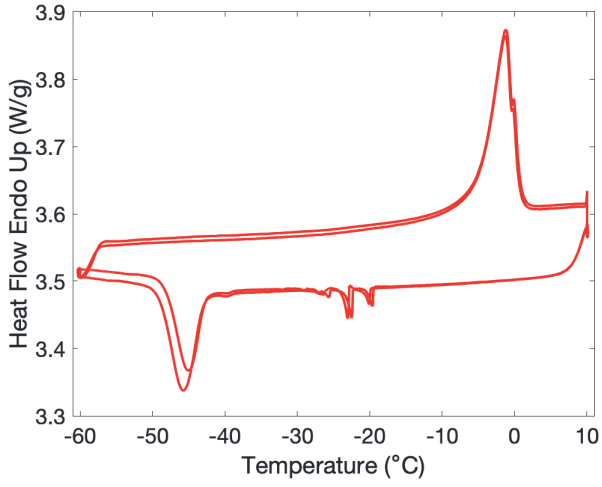

Figure 5.A.8 DSC thermogram of ZnO-LO-3 corrected for the sample weight (5.61 mg).

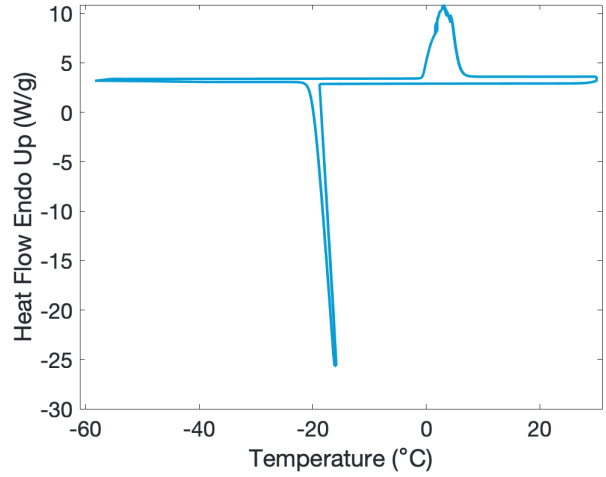

Figure 5.A.9 DSC thermogram of bulk deionised water corrected for the sample weight (5.5 mg).

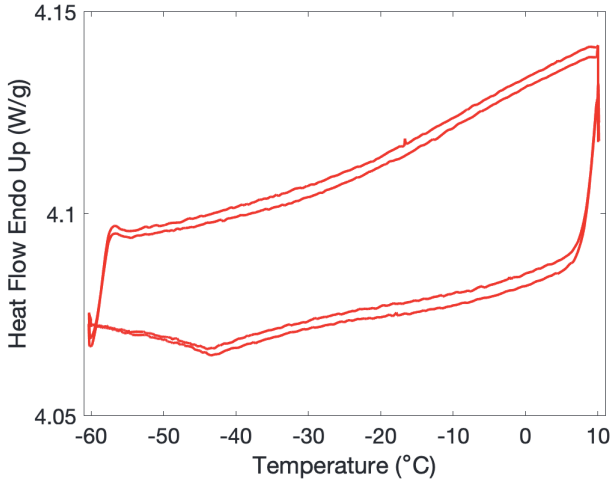

Figure 5.A.10 DSC thermogram of ZnO-LO conditioned at 90% RH corrected for the sample weight (4.94 mg).

Weight loss during DSC

Table 5.A.4 Weight loss during DSC measurements.

Sample name	ZnO-LO	TiO_2-LO	Zn-ionomer	ZnO-LO-2	ZnO-LO-3
Sample weight (mg)	5.67	5.83	4.71	5.51	5.61
Weight sample + DSC pan before measurement (mg)	55.50	55.55	54.88	54.88	55.17
Weight sample + DSC pan after measurement (mg)	55.42	55.53	54.87	54.87	55.14
Weight loss (%)	0.15	0.03	0.01	0.02	0.06

Transmission FTIR at room temperature

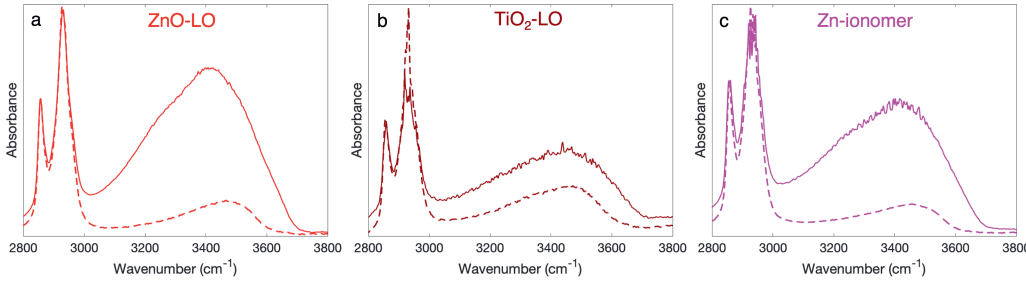

Figure 5.A.11 Transmission FTIR spectra showing the OH stretch band of saturated paint film (continuous line) and dried paint film (dashed line) (1 minute at 130 °C) for ZnO-LO (a), TiO_2-LO (b) and Zn-ionomer (c). Normalisation on ν_s (CH) CH_2 at 2859 cm^{-1}. The alcohol contribution is estimated from the ratio of the integrated OH stretch band of the dried film compared to the saturated film. The estimated alcohol contribution corresponds to 18%, 56% and 20% for ZnO-LO, TiO_2-LO and Zn-ionomer, respectively.

5.B Appendix 2

DSC thermograms of paint films with different pigmentation

Paint films were prepared by mixing linseed oil (LO) (Kremer Pigmente, from Sweden, cold-pressed, low acid content) with pigments using a glass muller on a glass slab. Paint films were cured in the dark at 60 °C at 12% RH for 1 week. DSC measurements were executed according to the method described in the Materials and Methods of Chapter 5, unless stated otherwise. The DSC run was cycled twice between -60 and 30 °C, unless stated otherwise.

Minium (Pb_3O_4) (Sigma Aldrich, 99% purity) in linseed oil 3:1 w/w was prepared in September 2020, DSC was performed September 2022. To prepare lead ionomer model system, 0.12 g lead sorbate was added to 0.8 g LO. Lead sorbate was synthesised according to Baij et al. 2018 [25]. Lead ionomer model systems were prepared February 2017, DSC was performed September 2022. Carbon black-LO films were prepared in December 2023, DSC was performed January 2024. 0.52 g carbon black (Kremer Rebschwarz reines Pflanzenschwarz Deutsch) was mixed with 0.5 mL LO. Iron oxide-LO films were prepared in December 2023, DSC was performed January 2024. 0.53 g red iron oxide (120 M, synthetic iron oxide >3 nm, Kremer Pigmente) was mixed with 0.5 mL LO.

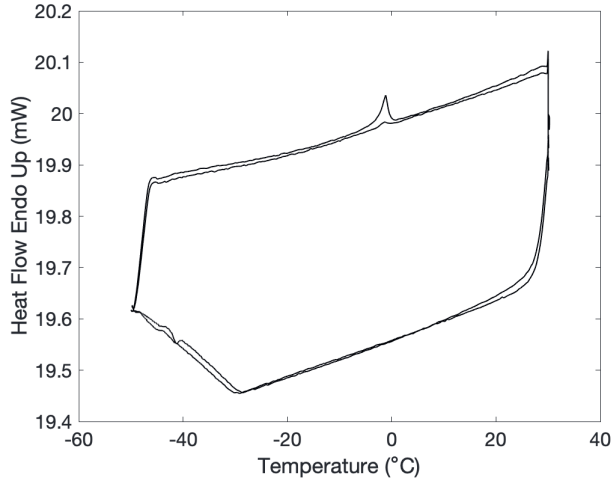

Figure 5.B.1 Thermogram of water-saturated minium oil paint.

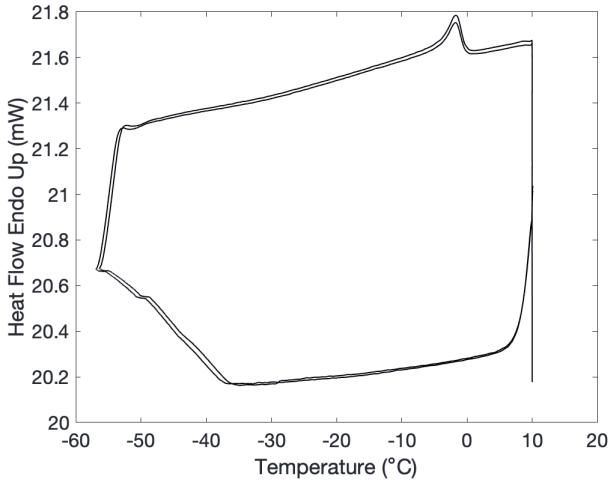

Figure 5.B.2 Thermogram of water-saturated carbon black oil paint.

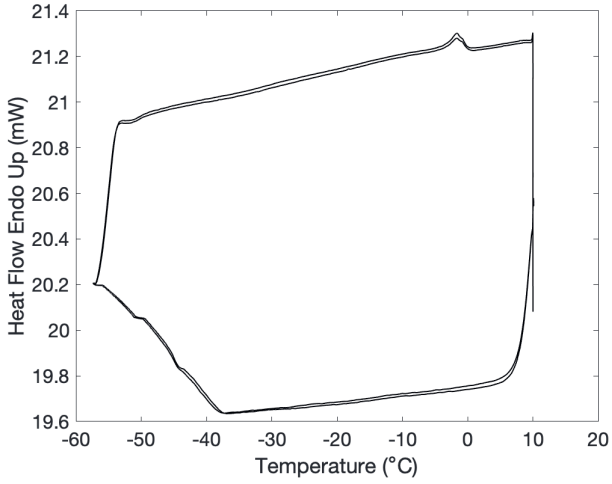

Figure 5.B.3 Thermogram of water-saturated iron oxide oil paint.

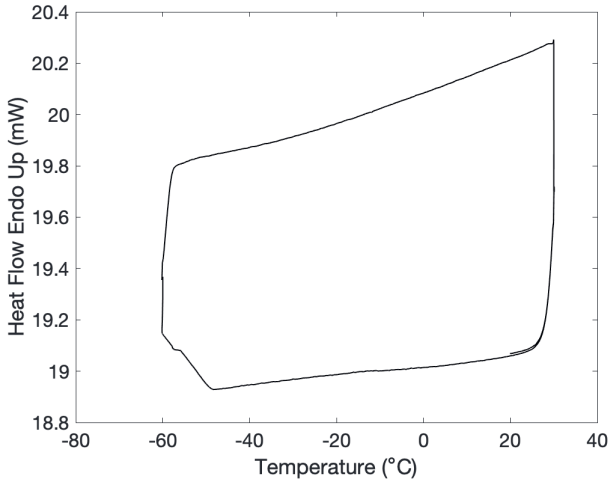

Figure 5.B.4 Thermogram of water-saturated lead-ionomer. DSC run was cycled once between -60 and 30 °C.

Quantification of ratio freezable to nonfreezable water

The following methodology was developed to determine the ratio between freezing and non-freezing water in paint films. Paint films were prepared on glass slides with known weights in the same way as described in the Materials and Methods of Chapter 5 in triplicate. After curing, the paint films including their glass support were placed in a closed contained with silica gel. After 2 days, the dry weight of the paint films was recorded. Paint films including glass support were subsequently placed in deionised water for 4-5 days. The paint films and glass support were patted dry, and their wet weight was recorded while covered with a second glass slide with known weight to avoid evaporation. Subtracting the dry weight from the wet weight gives the water content (mg).

A piece (± 5 mg) of the wet paint film was cut and placed into a sealed aluminum DSC pan. DSC runs were performed according to the method described in Chapter 5. The melting peak was integrated (**Figure 5.B.5**). Dividing the peak area (in mJ) by the latent heat of water at 0 °C (333.5 J/g) gives the amount of freezable water in mg. Subtracting the amount of freezable (F) water from the total moisture content gives the amount of nonfreezable (NF) water in mg.

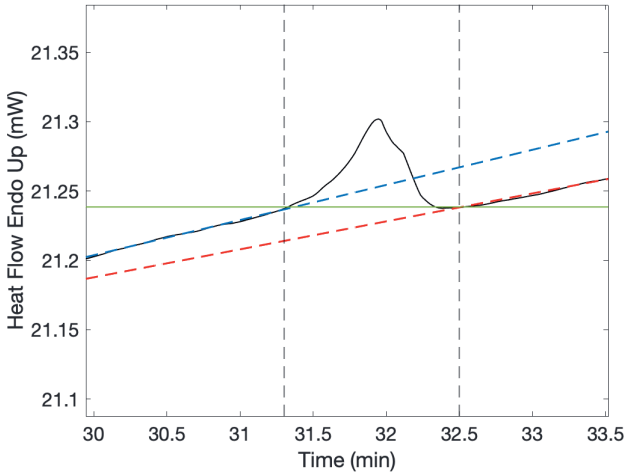

Figure 5.B.5 Example of integration boundaries. Two linear baselines are manually selected that indicate the slope before (blue dashed line) and after the peak (red dashed line). The onset and end of the peak are defined as the points where the thermogram diverges from the baselines (black vertical dashed lines). A linear baseline is drawn between the onset and the end for integration (green line).

For three types of paint (water-saturated zinc oxide, carbon black and iron oxide linseed oil paint, all 1:1 w/w pigment:oil) this methodology has been followed to find the ratio freezing to non-freezing water. The results of the gravimetric part are presented in **Table 5.B.1**. The results are based on measurements performed in triplicate. The moisture content in wt% is compared to the moisture content determined with DVS on paints with the same composition (not the same set). DVS measurements were done following the method described in Chapter 5.

Table 5.B.1 Moisture content of water-saturated iron oxide, carbon black and zinc oxide oil paint determined by gravimetry and DVS.

Paint/sample	Dry weight (mg)	Wet weight (mg)	Water content (mg)	Water content (wt%)	Water content at 95% RH (DVS)
Iron oxide-LO 1	0.5471	0.5536	0.0066	1.213	
Iron-oxide-LO 2	0.5754	0.5818	0.0066	1.142	
Iron-oxide-LO 2	0.3168	0.3209	0.0045	1.143	
Iron oxide-LO				**1.26 (SD = 0.15)**	**2.92**
Carbon black-LO 1	0.3702	0.3809	0.0115	3.113	
Carbon black-LO 2	0.4781	0.4917	0.0148	3.103	
Carbon black-LO 3	0.4091	0.4209	0.0125	3.069	
Carbon black-LO				**3.10 (SD = 0.02)**	**4.45**
Zinc oxide-LO 1	0.2397	0.2453	0.0057	2.393	
Zinc oxide-LO 2	0.4419	0.4522	0.0106	2.393	
Zinc oxide-LO 3	0.4489	0.4588	0.0102	2.281	
Zinc oxide-LO				**2.36 (SD = 0.06)**	**3.61**

Table 5.B.1 shows that the gravimetric method yields values for moisture content with a low standard deviation. However, the moisture content determined by gravimetry is consistently lower than the moisture content at 95% RH determined by DVS. It is expected that the moisture content at 95% RH is lower than that in saturated samples. Our hypothesis for the lower water content obtained by gravimetry of saturated samples compared to DVS is that polar material leaches out of the paint films when left in water for a few days. That would mean that the total weight of the samples goes down and that we currently underestimate the amount of water in the paint films.

Table 5.B.2 presents the results of the analysis of the thermograms. The total water content of the DSC samples is calculated by multiplying the sample weight with the relative water content (in wt%) found with gravimetry. The obtained fraction F/(F+NF) indicates that only a small portion of water present in these oil paints is freezable, and therefore clustered. If we consider that the total water content in the films is underestimated with the gravimetric method, the true percentage of freezable water should be lower. The freezable water fraction presented here, therefore, should be interpreted as the upper limit. Finally, there is a noticeable difference in melting peak position between ZnO-LO and the other two paints. Freezable water in ZnO-LO melts at a temperature more than 2 °C lower. This observation suggests that the size of freezable water clusters can vary between paints with different pigments.

Table 5.B.2 Analysis of DSC thermograms to calculate freezable (F) and nonfreezable water (NF) in water-saturated iron oxide, carbon black and zinc oxide oil paint.

Paint/DSC run	Sample weight (mg)	Total water content (mg)	Peak position (max.) (°C)	Peak area (mJ)	Freezable water (F) (mg)	Non-freezable water (NF) (mg)	Fraction F/(F+NF)
Iron oxide-LO cycle 1			-1.6	1.63	0.005		
Iron oxide-LO cycle 2			-1.6	1.44	0.004		
Iron oxide-LO	9.035	**0.114**			**0.005**	**0.109**	**0.04**
Carbon black-LO cycle 1			-1.7	4.62	0.014		
Carbon black-LO cycle 2			-1.8	4.57	0.014		
Carbon black-LO	6.397	**0.198**			**0.014**	**0.184**	**0.07**
Zinc oxide-LO cycle 1			-3.9	6.54	0.020		
Zinc oxide-LO cycle 2			-4.0	6.29	0.019		
Zinc oxide-LO	7.897	**0.186**			**0.020**	**0.166**	**0.11**